A Dual Radiometer System for Traffic Monitoring

Mario Leib[1], Muhammad Fahad Khan[2], Winfried Mayer[1] and Wolfgang Menzel[1]

[1] *University of Ulm, Microwave Techniques, Albert-Einstein-Allee 41, 89081 Ulm, Germany*
[2] *now with: Mobilink GSM, Karachi, India*

Email: mario.leib@uni-ulm.de

***Abstract*— In this paper a experimental radiometer setup is presented consisting of two identical total power radiometers operating at 38 GHz. This setup can be used for traffic density monitoring and velocity measurement of vehicles. A vehicle is detected by the radiometer sensor due to the temperature difference between the vehicle and the ambient temperature, where the different temperature characteristics by the vehicle are caused by reflections of the low sky temperature. The velocity of a vehicle passing the system is calculated by the measured time period needed by the vehicle in order to pass the two radiometer sensors using a correlation function between the two responses. Within this paper a brief description of the realized sensor system and first characteristic measurements are shown. The results demonstrate the functionality of this novel concept.**

I. Introduction

As the traffic density increases year by year, it is useful to have information about the traffic flow on the streets. Then, in long-term, the traffic could be regulated by a different traffic routing. Further, it is desirable to regulate the traffic at e. g. traffic jam critical locations like gateways. If the street before a gateway is equipped with the described sensor, then information about the vehicles' speed and the traffic density can be obtained. These data can be used to predict possible traffic jam situations and to avoid them in some cases by the adaption of the speed limits in front of the gateway [1] or by a gateway control [2], e. g. by a traffic light which allows vehicles to enter the highway in certain time steps depending on the traffic density on the highway.

Beside the use for traffic classification and regulation this sensor can, especially due to its flexibility, also be applied for traffic speed observation. According to police reports speeding is a main reason for road accidents. Therefore, velocity controls are mandatory in order to ensure that everybody drives with a speed adapted to the road conditions. Obviously, there are already several established sensors existing for velocity control like CW-radars, light barrier systems, induction loops and laser sensors. But the presented sensor combines several advantages of these existing systems. So, for example, unlike radar sensors, this technology is completely passive, therefore no warning systems can be applied and, compared to a simple light barrier, no receivers on the street side opposite to the sensor are necessary avoiding a dangerous crossing of the street for the operating personal. However, the velocity information has to be much more accurate for this application.

II. Measuring Principle

A radiometer measures the emitted noise power of a object within the beam of the radiometer's antenna. For a "black body", i. e. an absorbing object, this power is proportional to the temperature of the object according to Eq. 1.

$$U \propto P = kT\Delta f, \tag{1}$$

where k is the Boltzmann constant, T the object temperature and Δf the frequency bandwidth of the radiometer. When a vehicle passes one of the radiometer's antennas a significant signal change can be recorded as already demonstrated in [3] and depicted in Fig. 1. This temperature signature is not caused by the temperature of the vehicle itself, because the metallic car body is, in a radiometric sense, a good reflector, but by the low sky temperature reflected into the radiometer antenna by the car body. Of course, the sky temperature is not constant and depends on the weather conditions, but a sufficient difference to the ambient temperature is always given. So a typical value for the clear sky temperature at 38 GHz is about 20 K [4], which is much lower than the ambient temperature. Hence, a vehicle can be detected.

The velocity measuring principle behind this new sensor system is equal to that of light barriers. But instead of two light barriers, two identical radiometers are directed towards the road with a certain distance between the sensors. When a vehicle is detected, the radiometer output voltages, corresponding to the temperature signature, of both sensors can be

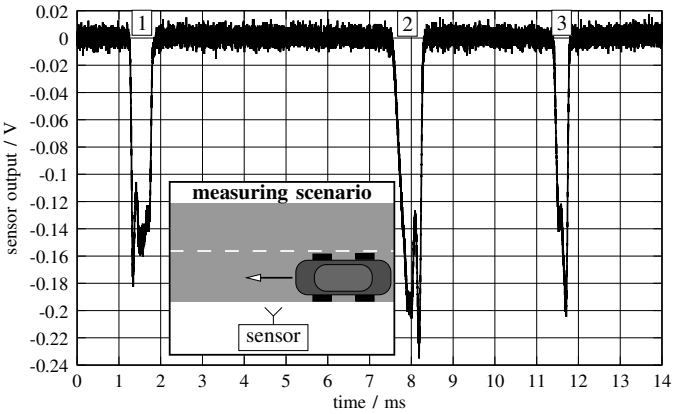

Fig. 1. Typical output of the radiometer sensor for three different vehicles passing the sensor ($U \propto P \propto T$, 0 V $\hat{=}$ 290 K).

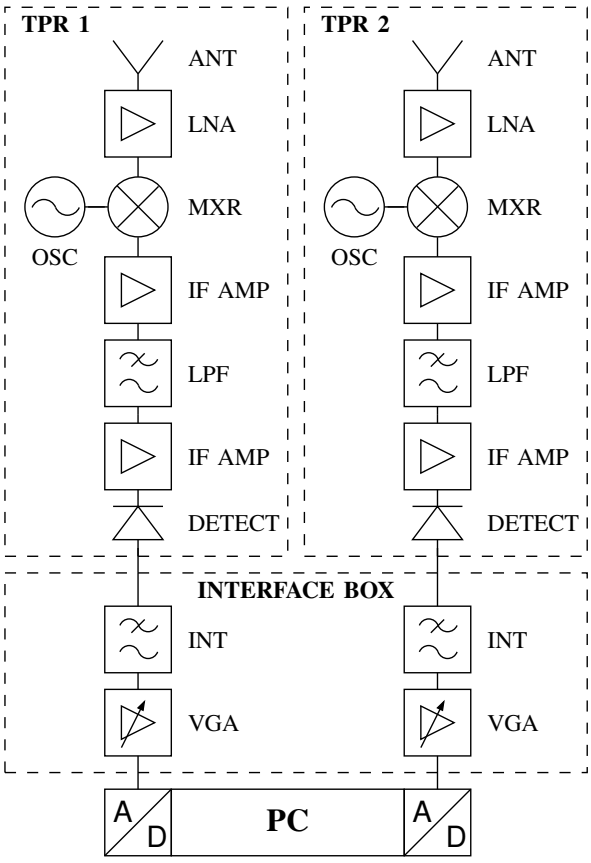

Fig. 2. Block diagram of the dual radiometer system.

recorded. Then, the time period τ_{vehicle} of a passed vehicle can be easily achieved by correlating the signals of the two sensors $s_1(t)$ and $s_2(t)$ (see Eq. 2). The position of the maximum value of the correlation function $x(\tau)$ corresponds to τ_{vehicle}.

$$x(\tau) = \sum_{t=-\infty}^{\infty} s_1(t) \cdot s_2(t+\tau) \tag{2}$$

Finally, the velocity of the vehicle can be calculated with the known distance between the two sensors.

III. The Dual Radiometer System

A. System Architecture

Figure 2 shows the block diagram of the developed dual radiometer system, which basically consists of two identical total power radiometers (TPR) [5]. Via an interface box, each TPR is connected to a commercially available analog-to-digital converter PCMCIA plug-in card for data acquisition, so the measured data can be stored and displayed online at a PC. Within the interface box integration of the obtained signals by a low-pass filter (INT) and adjustment of the amplitude of the two radiometer branches (VGA) is done.

Each TPR operates at a center frequency of 37.5 GHz and has a bandwidth of 1.8 GHz. The radiation power collected by the antenna (ANT) is amplified with a low-noise amplifier

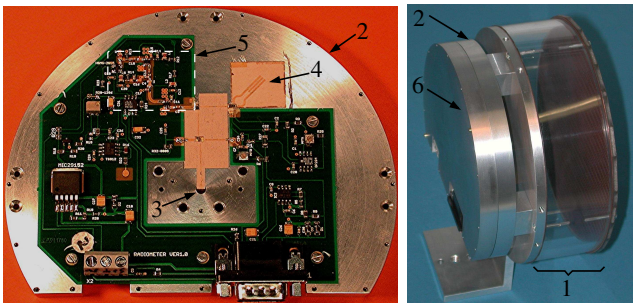

(a) Assembled circuitry base plate. (b) Side view of a sensor.

Fig. 3. Photographs of a realized radiometer sensor.

(LNA) and then down-converted. At the intermediate frequency (IF) stage the signal is further amplified by 40 dB with two amplifiers (IF AMP), and frequency band limitation is performed by a low-pass filter (LPF) with a cut-off frequency of 1 GHz. At lower frequencies an additional band limitation is done by the amplifier due to its transfer function. So the 1/f-noise is reduced, and a better overall noise figure can be achieved. Finally, a video signal is generated by a square-law detector (DETECT).

B. Sensor Hardware Realization

In order to be able to perform different test scenarios with different distances between the sensors, each TPR sensor is realized in a compact manner. In Fig. 3 a photograph of one completely assembled TPR and the mounted millimeter-wave (mmW) and IF stage circuits are shown.

Basic element of each sensor is the folded reflector antenna (1) with a beamwidth of 4° in azimuth and elevation and a side-lobe suppression of 19 dB [6]. The backside of the antenna serves as mount for the base plate (2) of the mmW, IF and electronic parts. At the center of the base plate, a microstrip-to-waveguide transition (3) is integrated, transforming the waveguide mode of the antenna feed into a microstrip mode [3]. Hence, the mmW components can be realized in microstrip technique, where RT Duroid 6010 with a height of 254 µm and a dielectric constant of $\epsilon_r = 10.2$ is used as substrate material. Due to this compact integration the transmission losses from the antenna to the LNA are kept small improving the temperature resolution of the TPR. As local oscillator of the down-converter, a voltage-controlled oscillator MMIC is used. An external microstrip resonator (4) determines the output frequency. A slight adjustment of the output frequency can be done by the varactor tuning voltage. All components of the IF stage (5), the power supply circuitry and the interface connectors are located on a single separate PCB with FR4 as base material. A housing (6) covers the circuit base plate for shielding purposes and protection of the MMICs. The overall performance of both realized TPR is summarized in table I. As can be seen, the noise figures differ slightly, which is supposed to be caused by production tolerances at the assembly process of the microstrip-to-waveguide transition and tolerances of the MMICs.

TABLE I

PERFORMANCE DATA OF THE REALIZED SENSORS.

Parameter	TPR1	TPR2
Center frequency f_0	37.5 GHz	
Bandwidth Δf	1.8 GHz	
Total gain G	49.7 dB	49.7 GHz
Noise figure F (without antenna)	7.1 dB	7.6 dB
Noise figure F (with antenna)	7.8 dB	8.3 dB
Integration time τ_{int}	0.6 ms	0.61 ms
Temperature resolution ΔT	2.4 K	2.6 K
Angular resolution $\theta_{3\,\text{dB}}$	4°	
Sampling rate f_{sample}	1 kHz	
Size (diameter/depth)	150 mm /85 mm	

IV. TEST RESULTS

A. Measurements at road side

In order to prove the concept of the realized dual radiometer system, first measurements were performed at road side. Thereby, both radiometer sensors were placed in parallel with a distance of 1 m between each other and about 6 m to the road (see Fig. 4). Furthermore, the height of the sensor was 1 m. The center of the antenna main beams are directed parallel to the ground towards the road. Due to the small antenna beamwidth of 4° only an area with a diameter of 50 cm is observed at the car body.

In Fig. 4 a picture of the measurement setup is depicted together with typically recorded measurement results for a car passing the sensor system. In the diagram in Fig. 4, the sensor output voltage is normalized manually such that zero volts equals the background temperature. A separate calibration has shown that 1 mV output voltage belongs to a temperature difference of about 0.5 K. Despite inconvenient conditions during the measurement with a low ambient temperature of −5°C (268 K) and a clouded sky, a significant voltage signature could be obtained when a car passed the sensor. Also, as expected, the recorded signatures for the two sensors have a very similar shape. In Fig. 5 the normalized correlation function of the two signals is shown. The position of the maximum for the road side measurement corresponds to the time delay of the vehicle and, using the known distance of the sensors, allows to calculate the velocity of the car. In the shown example the time delay is 123 ms yielding a velocity of 29.27 km/h. Several measurements with different car types have been performed showing the functionality of the detection concept. More measurements with different vehicles like trucks, buses and motorcycles are needed to collect more data about typical signatures. So one problem of the current setup is that the detection of a vehicle is coupled with a undershoot of a predefined threshold voltage. If this threshold voltage is too low than a vehicle with a low-reflective surface, like buses or trucks, will not be detected and no velocity will be calculated. Therefore, care has to be taken about the optimum threshold value and, of course, the calibration of the sensors itself.

In order to validate the accuracy of the velocity measurement a simple reference system by a laser light barrier has been build up. Some test trails have been performed, but due to the short test track, the maximum velocity was limited to about 50 km/h. These measurements resulted in a standard deviation of 1.001 km/h showing a good agreement between laser reference system and the radiometer setup. Of course, this accuracy does not qualify the system for traffic observation yet, but further investigations showed that the deviation is basically caused by an inaccuracy of the electronics of the reference system. Therefore, another verification with a more precise reference setup is necessary.

B. Measurements from a bridge

Beside the use at road side this system can also be applied from bridges, gantries and over-passes, where the sensor can be mounted perpendicular to the road surface like displayed in Fig. 6. In Fig. 7 the measurement result from a bridge for four cars is depicted. The distance between the sensors in the arrangement was 6.5 m and about the same ambient conditions existed like at the road side measurements.

Compared to the measurement results at the road side the recorded signatures are slightly unequal for the two sensors. Beside a possible misalignment of the radiometers, these inequality is caused mainly by the following effect. Due

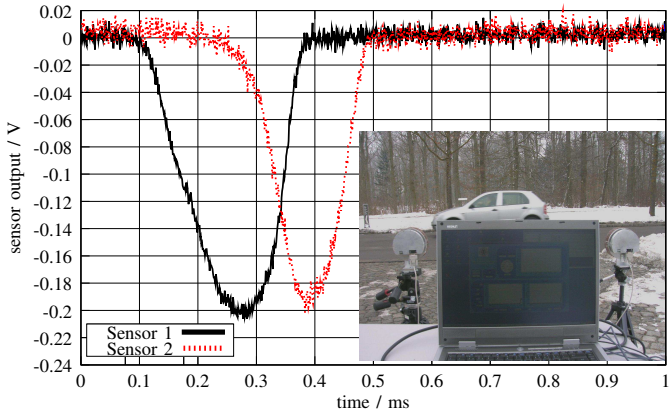

Fig. 4. Typical measured data for a car at the road side.

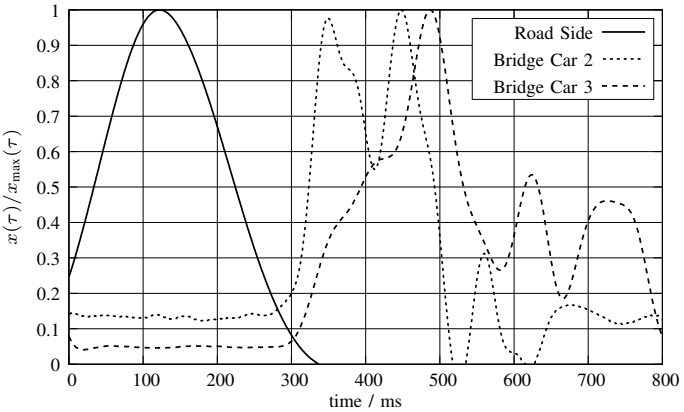

Fig. 5. Normalized correlation function for road side and bridge measurements (compare Fig. 4 and Fig. 7).

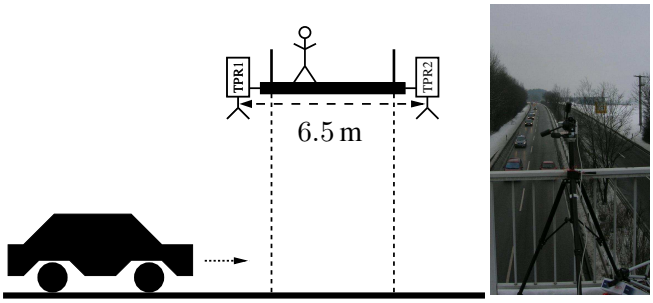

Fig. 6. Measuring setup for measurements from the bridge.

to the slanted surfaces of the car body the temperature of the bridge constructions are reflected in the antenna of the radiometers instead of the sky temperature. This leads to asymmetries in the signature, because for the first sensor the bridge constructions is seen in front of the car, and for the second sensor behind the car. Another interesting difference to the road side measurements are the notches within the signature of a car. These notches occur as the glass panels of the vehicles, like the front windshield, mainly do not have a reflective behavior. Therefore, the temperature of the vehicle interior instead of the sky is measured. This effect is clearly demonstrated by the second car in Fig. 7, as the glass roof results in a much less distinctive signature compared to vehicles with the metal roof.

Because of the asymmetrical signatures of the two sensors and the notches, the correlation function is less smooth compared to the road side result and even several distinctive peaks can occur (see Fig. 5, car 2), which could lead to a wrong velocity determination. But during the test measurements no false detection was noticed.

Unfortunately, no reference setup for the obtained velocities could be applied during the measurements from the bridge. Therefore no information about the accuracy of the results is possible. But as can be seen from Table II, the velocities of the vehicles out of Fig. 7 are quite similar, which is in accordance with the fact that they drove quite close to each other. Hence, at least the relative velocity difference seems

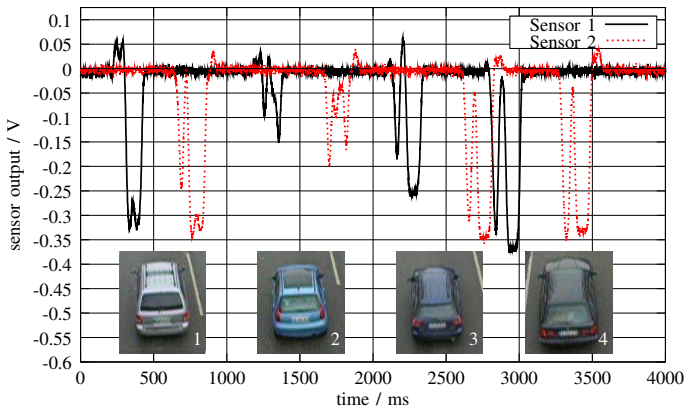

Fig. 7. Typical measurement results from a bridge for four different cars.

TABLE II
DETERMINED VELOCITIES FOR THE VEHICLES IN FIG. 7 .

Vehicle	τ[ms]	v[km/h]
1	429	54.55
2	447	52.35
3	487	48.05
4	479	49.47

to be reasonable. For further investigations of the velocity accuracy of the system from bridges a reference measurement with a CW-radar or a laser sensor is considered.

V. CONCLUSION

It has been shown that a radiometric sensor is capable of monitoring vehicles on a street and, in principal, the velocity of different vehicles can be obtained with the introduced dual radiometer system by correlation of the recorded temperature signatures. In addition, it has been demonstrated that the system can be applied both at the road side as well as from a bridge. Further effort has to be spent on the calibration process of the radiometer sensors, the velocity accuracy determination of the system with a more precise reference system, especially for measurements from an over-pass, and more data have to be recorded at different ambient conditions in order to approve the robustness of the system concept.

If the accuracy of the velocity measurements is certified, the system could be also used for the determination of the safety relevant information about speed and distance of vehicles. Additionally, the antenna beam shape could be easily optimized for certain applications like described in [7], in order to fit the beam shape to the geometries of the vehicles.

REFERENCES

[1] E. van den Hoogen, S. Smulders, and H. Advies;, "Control by variable speed signs: results of the dutch experiment," in *Road Traffic Monitoring and Control*, 1994, pp. 145–149.

[2] M. Treiber, A. Kesting, and D. Helbing, *Für eine neue deutsche Verkehrspolitik - Verkehr verstehen und beherrschen*. Deutscher Verkehrs-Verlag, 2005, pp. 76–85.

[3] W. Mayer, H. Bilzer, R. Leberer, A. Gronau, W. Menzel, and R. Müller, "Design and realization of a compact 38 GHz radiometer," *Frequenz*, vol. 57, no. 11-12, pp. 214–220, November/December 2003.

[4] F. T. Ulaby, R. K. Moore, and A. K. Fung, *Microwave Remote Sensing - Active and Passive*. Reading, USA: Addison-Wesley, 1981, vol. 1.

[5] M. E. Tiuri, "Radio astronomy receivers," *IEEE Transactions on Microwave Theory and Techniques*, vol. 12, pp. 930–938, Dec. 1964.

[6] W. Menzel and D. Pilz, "Printed quasi-optical mm-wave antennas," in *IEEE International Symposium on Antennas and Propagation*, vol. 38, July 2000, pp. 790–793.

[7] R. Leberer and W. Menzel, "Folded millimeter-wave shaped-beam reflectarrays," in *Topical Symposium on Millimeter waves (TSMMW)*, Mar. 2004, pp. 93–97.